Journal of Nuclear Materials 442 (2013) S229–S232
DOI: http://dx.doi.org/10.1016/j.jnucmat.2013.03.039

Microstructure and temperature dependence of the microhardness of W–4V–1La_2O_3 and W–4Ti–1La_2O_3

B. Savoini *, J. Martínez, A. Muñoz, M.A. Monge, R. Pareja

Departamento de Física, Universidad Carlos III de Madrid, 28911 Leganés, Spain

Abstract: W–4V–1La_2O_3 and W–4Ti–1La_2O_3 (wt.%) alloys have been produced by mechanical alloying and subse-quent hot isostatic pressing. Electron microscopy observations revealed that these alloys exhibit a submi-cron grain structure with a dispersion of La oxide nanoparticles. Large V or Ti pools with martensitic characteristics are found segregated in the interstices between the W particles of the respective alloys. Microhardness tests were carried out over the temperature range 300–1073 K in vacuum. The microhard-ness–temperature curve for W–4V–1La_2O_3 exhibited the expected decreasing trend with increasing tem-perature although the microhardness stayed constant between ~473 and 773 K. The W–4Ti–1La_2O_3 presented quite different temperature dependence with an anomalous microhardness increase for tem-peratures above ~473 K.

1. Introduction

The current He-cooled divertor concepts for the future demonstration fusion reactor (DEMO) are based on the use of pure W and W alloys because some of these materials could exhibit a more favourable combination of properties required for armour or structural material in plasma facing components (PFCSs) [1,2]. Favourable properties include high melting temperature, good thermal conductivity and creep strength, thermal shock resistance, minimal tritium retention, low sputtering and erosion rates, and resistance to damage from fusion neutrons. Nevertheless, W and W alloys are inherently brittle at low temperatures. According to the existing literature data, the reliable operating temperature window (OTW) for W materials in a PFC is between ~1073 and 1500 K [2]. The lower and upper bounds of this OTW are respectively defined by the ductile–brittle transition temperature (DBTT) and recrystallization temperature (RCT) of the material. The safety and efficiency of a fusion reactor will depend on the OTW-range. In particular, it would be compulsory to use W materials having a DBTT as low as possible and a suitable toughness and ductility at low temperatures, for preventing accidental brittle fracture when the PFCs are at temperatures below the lower bound of the OTW. Oxide reinforcement, or Al–K–Si doping, can enhance the mechanical strength of W and increase its recrystallization temperature, although without lowering the DBTT [3,4]. Recently, W–Ti and W–V alloys, reinforced or oxide dispersion strengthened (ODS) with Y_2O_3 or La_2O_3, have been produced by mechanical alloying and subsequent consolidation by hot isostatic pressing (HIP) [5–7]. It has been reported that the addition of Ti by itself, or combined with Y_2O_3, can moderately enhance the strength and fracture toughness of W in the temperature range below ~873 or 1073 K, and noticeably enhance microhardness [8,9]. However, these results did not show an apparent decrease of the DBTT. In the case of W–Ti alloys, the formation of some metastable Ti phase (α', α'' or ω) could impair the mechanical behavior of W–Ti alloys. However, because W–V alloys have an isomorphous phase diagram with a continuous range of solid solution, similar impairment is not expected to occur. Further, the potential of W–V composites as a wide OTW material for high-temperature applications has been investigated by numerical simulation. Simulation results, and preliminary toughness and creep measurements performed on a trial W–V composite, suggest a plausible capability of V to improve the mechanical characteristics of W at low temperatures [10]. Also, it is noteworthy that Y_2O_3 addition to W–V alloys appears to inhibit the growth of grains having sizes larger of ~1 μm [11].

This paper reports the results of the microstructural studies and microhardness tests at elevated temperature performed on W–4V–1La_2O_3 and W–4Ti–1La_2O_3 (wt.%) alloys in an attempt to explore the potential of this type of ODS W alloys for fusion applications. Hereafter the alloys will be referred to as W–4VLa and W–4TiLa.

2. Experimental procedure

The alloys were prepared from W, V, Ti, and La_2O_3 powders with purity and particle sizes of 99.9% and <5, 99.5% and 41, 99.9% and 110 μm and 99.5% and <50 nm, respectively. The powders were

* Corresponding author. Address: Departamento de Física, Universidad Carlos III de Madrid, Avda. Universidad Carlos III de Madrid 30, 28911 Leganés, Spain. Tel.: +34 916249413; fax: +34 916248749.

E-mail address: begona.savoini@uc3m.es (B. Savoini).

processed and consolidated in four stages: (1) blending of the starting powders in a Turbular T2F mixer for 4 h; (2) mechanical alloying of the powder blends in a high-energy planetary ball mill; (3) encapsulation and degassing for 24 h at 673 K; and (4) sintering by HIP for 2 h at 1573 K and 195 MPa. The mechanical alloying was carried out under a high purity Ar atmosphere in a pot lined with tungsten carbide (WC), using WC balls of 10 mm in diameter as grinding media at a ball-to-powder ratio of 4:3. Mechanical alloying of the blends were performed at a constant rate of 400 rpm using milling times of 10, 20 and 30 h. 10 h for W–4VLa and 30 h for W–4TiLa were adopted as a compromise milling time for constraining the O and C contamination and producing the suitable homogenization, refinement and morphology of powders that were HIP consolidated. The C and O contents in the powders in the as-blended and as-milled conditions, determined using LECO TC500 and CS-200 elemental analyzers, are given in Table 1 along with their O content excess. The O excess has been estimated by subtracting the stoichiometric O amount in the added La_2O_3 fraction from the measured O contents in the powders. Precise density measurements of the consolidated samples were carried out in a He ultrapycnometer. The density of the consolidated alloy resulted in ~98% (W–4VLa) and ~100% (W–4TiLa) of the theoretical density calculated applying the mixture rule.

Microstructural characteristics were investigated by X-ray diffraction (XRD) and scanning electron microscopy (SEM). XRD patterns were analyzed by the Rietveld method using the Fullprof software. Vickers microhardness measurements in the temperature range 295–1073 K were performed in vacuum applying a load of 4.9 N for 20 s. These tests were carried out in a high temperature microhardness tester using a sapphire indenter. The indentations were made starting from the highest temperature, after maintaining the sample temperature constant for 10 min. A minimum of six indentations were performed at each temperature.

3. Results and discussion

The SEM images of powders milled showed coarse flaky particles apparently formed by welding of stretched particles (see Fig. 1). Energy dispersion spectroscopy (EDS) analyses and electron backscattering (EBS) images evidence a homogeneous composition over the samples of the milled powder. However, inside these flaky particles could be detected evidences for undissolved V and Ti frequently embedded in the form of small filaments. Diffraction peaks corresponding to V, Ti or La_2O_3 were evident in the XRD patterns of the blended powders but undetected in the patterns of the milled powders, as Fig. 2 shows. Furthermore, a significant broadening of the XRD peaks of the milled powder can be observed. The average crystallite size and cumulative microstrain estimated from the width of the XRD peaks were: 129.6 nm and 0.39% for 10 h milled W–4VLa, 29.0 nm and 0.56% for 20 h milled W–4TiLa, and 26.8 nm and ~0.90% for 30 h milled W–4TiLa. The O excess in the milled powder rose significantly increasing the milling time from 10 to 30 h.

SEM analyses revealed that the HIP treatment produced the segregation of some V or Ti into large pools of these elements sparsely distributed in the corresponding alloy [6,7]. Fig. 3 presents element mapping images showing the La, V, Ti, and W distribution in the consolidated alloys. La is homogeneously and finely dispersed in the W matrix, while V and Ti tend to be localized in interstitial regions between the W particles. The Ti and V content inside the matrix, i.e. in areas free of pools, was found to be 3.6 and 3.1 wt.%, respectively. These values are very close to the nominal ones,

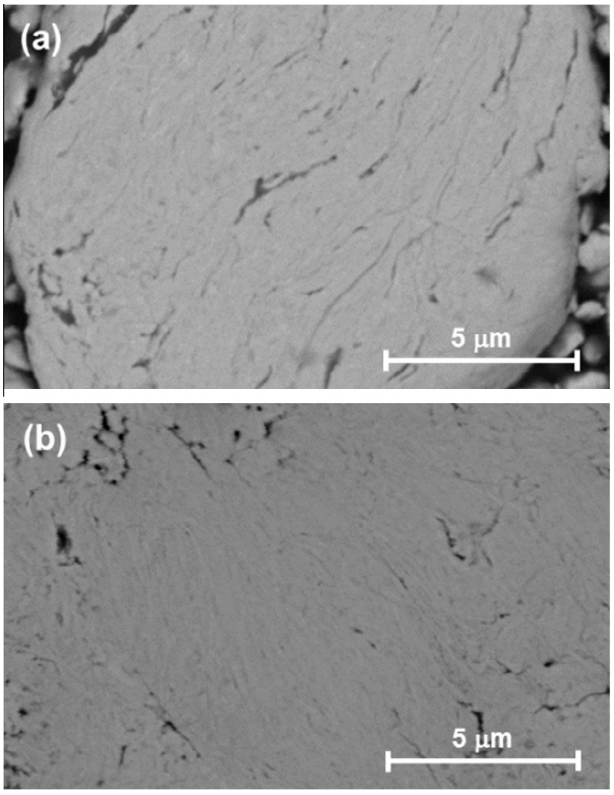

Fig. 1. SEM images of (a) W–4V–1La_2O_3 and (b) W–4Ti–1La_2O_3 milled powders.

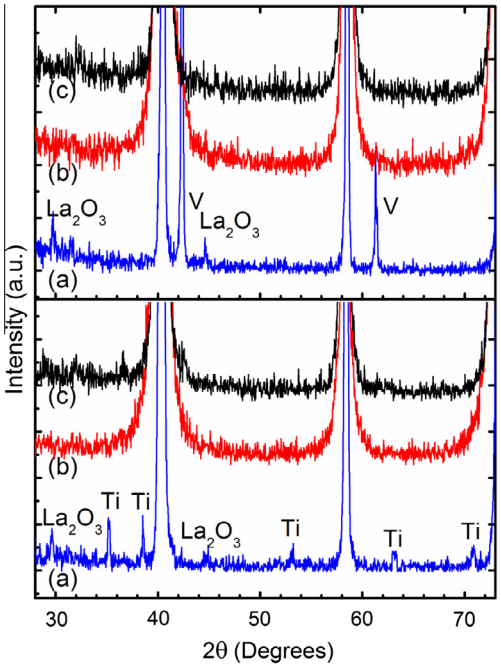

Fig. 2. XRD patterns for (a) blended, (b) milled and (c) HIP consolidated W–4V–1La_2O_3 (upper) and W–4Ti–1La_2O_3 (bottom).

Table 1
C and O content in the W–4VLa and W–4TiLa powders.

Content (wt.%)	W–4VLa		W–4TiLa	
	Blended	Milled	Blended	Milled
C	0.0358	0.0350	0.0338	0.0594
O	0.524	0.663	0.412	0.690
O excess	0.257	0.396	0.145	0.423

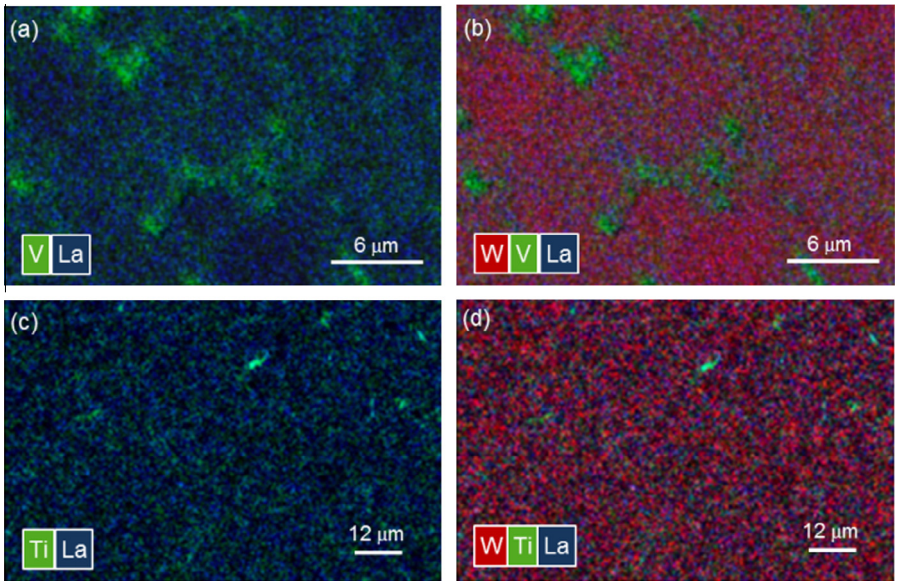

Fig. 3. Element map images showing the distribution of the alloying elements in (a) and (b) for W–4V–1La_2O_3, and (c) and (d) for W–4Ti–1La_2O_3.

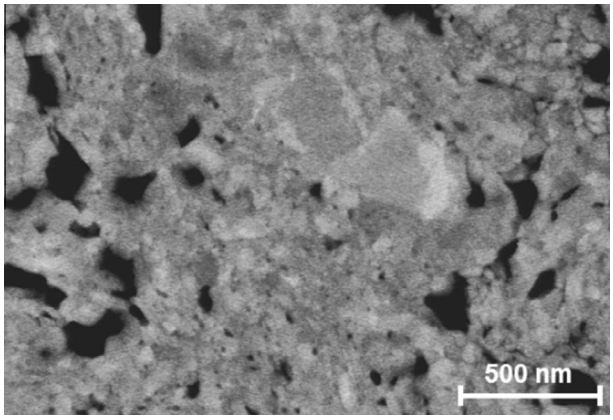

Fig. 4. ECC image showing the grain structure and the dispersion of particles with sizes smaller than ~25 nm in the W–4Ti–1La_2O_3 alloy. The irregular areas with sizes larger than ~0.2 μm are identified as Ti phase.

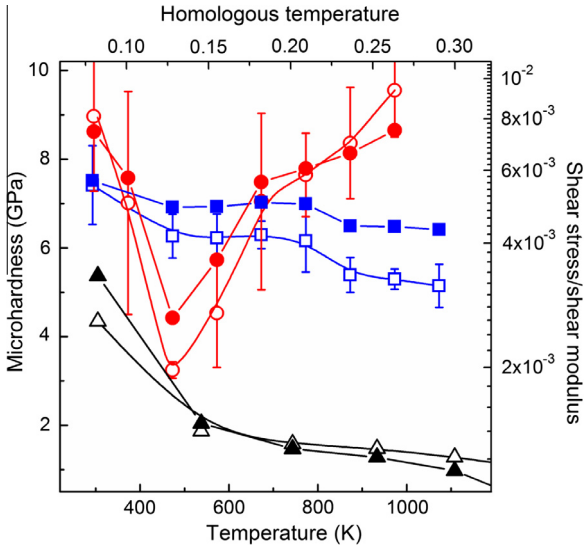

Fig. 5. Microhardness values (open symbols) and shear stress normalized to the shear modulus (solid symbols) as a function of temperature for W–4V–1La_2O_3 (squares) and W–4Ti–1La_2O_3 (circles). The values for work hardened W are also shown for comparison (triangles).

indicating that the amount of segregated Ti and V forming pools is low. This would explain why diffraction peaks attributable to V or Ti are not detected in the consolidated alloys.

Both consolidated alloys exhibited a submicron-grained structure and the presence of a fairly homogeneous dispersion of La-rich particles with sizes <30 nm as the electron channeling contrast (ECC) image for W–4TiLa in Fig. 4 reveals; the evidences of dispersion in W–4VLa has been reported elsewhere [7]. The nanometric characteristics of this dispersion have been also confirmed by small angle neutron scattering measurements [12]. Precise analyses of these La oxide particles to establish their composition and crystallographic structure in both alloys are in progress and not reported here.

Fig. 5 shows microhardness values for the alloys as a function of test temperature, along with hardness values for work-hardened W extracted from Ref. [13]. While the hardness for work-hardened W follows the expected temperature dependence due to thermally activated dislocation slip (i.e. a negative dependence), the alloys exhibit very different microhardness-temperature curves.

To compare the results with the deformation-mechanism maps, the H_V values were transformed into tensile yield strength values, σ_y, assuming the relationship $H_V \cong 3\sigma_y$, and then into shear stress values using the corresponding average Taylor factor $M = 2.73$ relating shear stresses to tensile stresses, and normalized to the shear modulus of W at the testing temperature. The resulting values are represented in Fig. 5 as a function of the homologous temperature. The shear modulus values for W as a function of temperature were obtained from the results reported in Ref. [14].

The W–4VLa presents a plateau with a constant microhardness of 6.2 ± 0.5 GPa in the temperature range ~473–773 K, which suggests a low-temperature deformation mechanism apparently limited by discrete obstacles, according to the deformation-mechanism map for W with grain size of 1 μm reported in Ref. [15]. These obstacles might be associated with the La-oxide dispersion since V dissolved in W does not produce strengthening. It should be noted that the atomic radius for V is significantly smaller than that of W. Above ~800 K this strengthening starts to wane (5.1 ± 0.5 GPa at

1073 K) and low-temperature deformation by thermally activated dislocation slip would be operative. In contrast, the microhardness curve for the W–4TiLa alloy reflects a quite different temperature behavior. After the initial decrease from 9.0 ± 1.7 to 3.2 ± 0.2 GPa, the microhardness increases noticeably for temperatures above 473 K up to 9.6 ± 1.1 GPa at 973 K. This microhardness behavior reveals an unexpected thermal hardening. It should be mentioned that the W–4%Ti and W–4%Ti–0.5%Y_2O_3 alloys processed under the same conditions exhibit an increase of the bending strength in this temperature range [9]. The observed thermal hardening should be attributed to a Ti effect rather than to an effect of the La_2O_3 addition because it is not observed in W–4VLa. However, no explanation can presently be offered by the authors for this hardening in the light of the present results. It should be noted that the surface of the V and Ti pools in these alloys exhibit relief that has been attributed to martensite plates [7]. The presence of a martensitic phase in the V and Ti pools in the alloy might be related to the observed hardening. The thermal expansion coefficients for V and Ti are almost twice the coefficient for W. These large mismatches would result in internal stresses in the pools induced by temperature changes, which can trigger local martensitic transformations in the pools and have effects on the mechanical behavior of these alloys.

4. Conclusions

The W–4VLa and W–4TiLa alloys processed by mechanical alloying and subsequent HIP exhibited a submicron grain structure with a dispersion of La oxide nanoparticles. Large pools of V or Ti were found segregated in the interstices between W particles. These pools showed martensitic characteristics and cracks that appear to have been induced by the thermal stresses induced by temperature changes.

The temperature dependence of the microhardness for these alloys reveals distinct behaviors. The W–4VLa alloy shows a decreasing trend of the microhardness with increasing temperature, but maintaining the microhardness values constant over the temperature range ~473–773 K. In contrast, the W–4TiLa alloy presents an anomalous microhardness increase for temperatures above 473 K.

The preliminary toughness and bending tests performed on these alloys have not revealed a significant enhancement of the mechanical properties [16] even although the present processing conditions appear to develop a particle dispersion and fine grain structure. This result could be associated to detrimental effects of the V and Ti segregation into the W particle interstices. Thus, other processing conditions, or routes, that can inhibit the V and Ti segregation should be explored in order to clarify the real potential of a rare-earth oxide dispersion for improving the W–V and W–Ti alloys. For instance, the content of V or Ti could be lowered below 1 wt.%.

Acknowledgements

The hardness measurements were carried out at the Materials Department of Oxford University. The authors express their gratitude to Prof. S.G. Roberts. This investigation was supported by the Spanish Ministry of Economy and Competitiveness (project ENE2012-39787-C06-05), the Comunidad de Madrid through the program ESTRUMAT-CM (Grant S2009/MAT-185), and the European Commission through the European Fusion Development Agreement.

References

[1] H. Bolt, V. Barabash, W. Krauss, J. Linke, R. Neu, S. Suzuki, N. Yoshida, ASDEX Upgrade Team, J. Nucl. Mater. 66 (2004) 329–333.
[2] P. Norajitra, L.V. Boccaccini, E. Diegele, V. Filatov, A. Gervash, R. Giniyatulin, S. Gordeev, V. Heinzel, et al., J. Nucl. Mat. 329–333 (2004) 1594–1598.
[3] M. Rieth, B. Dafferner, J. Nucl. Mat. 342 (2005) 20–25.
[4] M. Faleschini, H. Kreuzer, D. Kiener, R. Pippan, J. Nucl. Mat. 367–370 (2007) 800–805.
[5] M.A. Monge, M.A. Auger, T. Leguey, Y. Ortega, L. Bolzoni, E. Gordo, R. Pareja, J. Nucl. Mat. 386–388 (2009) 613–617.
[6] A. Muñoz, M.A. Monge, B. Savoini, M.E. Rabanal, G. Garcés, R. Pareja, J. Nucl. Mat. 417 (2011) 508–511.
[7] J. Martínez, B. Savoini, M.A. Monge, A. Muñoz, R. Pareja, Fus. Eng. Des. 86 (2011) 2534–2537.
[8] M.V. Aguirre, A. Martín, J.Y. Pastor, J. LLorca, M.A. Monge, R. Pareja, J. Nucl. Mater. 417 (2011) 516–519.
[9] M.V. Aguirre, A. Martín, J.Y. Pastor, J. LLorca, M.A. Monge, R. Pareja, J. Nucl. Mater. 404 (2010) 203–209.
[10] J. Hohe, P. Gumbsch, J. Nucl. Mater. 400 (2010) 218–231.
[11] J. Martínez, B. Savoini, M.A. Monge, A. Muñoz, R. Pareja, Fus. Eng. Des. Unpublished results.
[12] A. Muñoz, J. Martínez, M.A. Monge, B. Savoini, R. Pareja, A. Radulescu, Int. J. Refract. Met. Hard Mater. 33 (2012) 6–9.
[13] E. Lassner, W.D. Schubert, Tungsten, Kluwer Academic, New York, 1999. p. 21.
[14] V.M. El'kin, V.N. Mikhailov, T.Yu. Mikhailova, Phys. Met. Metallogr. 112 (2011) 535–548.
[15] H.J. Frost, M.F. Ashby, Deformation-Mechanism Maps, Pergamon Press, Oxford, 1982. p. 30.
[16] T. Palacios, J.Y. Pastor, M.V. Aguirre, A. Martín, M.A. Monge, A. Muñóz, R. Pareja, J. Nucl. Mater. 442 (2013) S277–S281.